Published in final edited form as:
Nanotoxicology. 2009 ; 3(3): 202–214. doi:10.1080/17435390902859556.

Gastrointestinal biodurability of engineered nanoparticles: Development of an *in vitro* assay

PAIGE N. WIECINSKI[1], **KEVIN M. METZ**[2], **ANDREW N. MANGHAM**[3], **KURT H. JACOBSON**[4], **ROBERT J. HAMERS**[3], and **JOEL A. PEDERSEN**[1,2,4,5]

[1]Molecular and Environmental Toxicology Center, University of Wisconsin, Madison, WI, USA

[2]Environmental Chemistry and Technology Program, University of Wisconsin, Madison, WI, USA

[3]Department of Chemistry, University of Wisconsin, Madison, WI, USA

[4]Department of Civil and Environmental Engineering, University of Wisconsin, Madison, WI, USA

[5]Department of Soil Science, University of Wisconsin, Madison, WI, USA

Abstract

The toxicity of engineered nanoparticles is expected to depend in part on their stability in biological systems. To assess the biodurability of engineered nanomaterials in the human digestive system, we adapted an *in vitro* assay previously used to evaluate the bioaccessibility of metals in contaminated soils. The compositions of the simulated gastric and intestinal fluids, temperature and residence times were designed to closely mimic conditions in the stomach and duodenum of the small intestine. We demonstrated the utility of the assay using $CdSe_{core}/ZnS_{shell}$ quantum dots functionalized with polyethylene glycol (PEG) thiol of two different molecular masses (PEG_{350} and PEG_{5000}). Under gastric conditions, removal of the PEG ligand diminished the stability of PEG_{350}-quantum dot suspensions, while PEG_{5000}-quantum dots were severely degraded. Inclusion of the glycoprotein mucin, but not the digestive protein pepsin, in simulated gastric fluids provided both PEG_{350}- and PEG_{5000}-coated quantum dots partial protection from transformations induced by gastric conditions.

Keywords

gastrointestinal biodurability; ingestion; quantum dot; exposure assessment; degradation; mucin

Introduction

A variety of government agencies and industry groups have expressed concern about the potential adverse impacts of nanotechnology, but remain optimistic that research on the biological effects of nanomaterials will influence the design of nanocomposites, devices incorporating them, and disposal strategies to minimize potential for undesirable environmental health and safety effects (NNI, 2006; EPA, 2007; ICF, 2006; Dunphy et al.,

Correspondence: Joel A. Pedersen, Dept. of Soil Science, University of Wisconsin, Madison, WI 53706-1299, USA. Fax +01 608 265 2595. japedersen@soils.wisc.edu.

2006). Exposure to engineered nanoparticles can occur via a variety of routes (e.g. ingestion, inhalation, dermal, intravenous). Oral exposure can be anticipated to occur through direct (e.g. drug delivery), incidental (e.g. water, food) or indirect (e.g. clearance from the lungs) routes given current and prospective applications of nanoparticles (Center for science, technology and public policy workshop, 2006). The biodurability of nanoparticles in the gastrointestinal tract (GI) is expected to affect uptake and potential toxicity of such materials.

The durability of engineered nanomaterials in biological systems is important for both therapeutic and diagnostic applications, as well as for inadvertent exposure, due to its influence on the toxicity of nanomaterials. Gastrointestinal biodurability of engineered nanoparticles (NPs) becomes especially important when considering the development and design of NP drug delivery systems. The term “biodurabilty” (Plumblee et al., 2003), as used in pulmonary toxicology, generally refers to the rate of particle dissolution, disintegration or removal from the lungs (Maxim et al., 2006; Muhle and Bellmann, 1997). For the purposes of this paper, we employ the term biodurability as the dissolution and/or disintegration of a particle under biological conditions (Plumblee et al., 2003). Compared to the number of studies that examine the biodurability of particles in lung fluids, relatively few studies exist that examine durability under conditions representative of the gastrointestinal tract.

In vitro assays designed to examine nanoparticle biodurability have advantages over their *in vivo* counterparts in terms of cost and time (Ruby et al., 1999). Although not a replacement for *in vivo* studies, *in vitro* gastrointestinal assays provide a convenient platform for examining the potential biodurability of engineered nanoparticles. An *in vitro* approach can permit rapid determination of the effects of NP coatings on biodurability, allow screening of a large range of NPs, and yield insight into the factors controlling nanoparticle fate in the GI tract. Furthermore, ethical issues associated with using human and animal models can be avoided.

Loss of ligands from the surface of semiconductor nanocrystals at low pH has been suggested to increase toxicity if such particles were to be exposed to gastric fluids (Aldana et al., 2005). However, pH is not the sole factor warranting consideration for assessing gastrointestinal biodurability. GI fluids are composed of a variety of constituents that could conceivably impact nanomaterial biodurability. In the fasted state, the human stomach has the following average composition: pH = 2.9, $[Na^+]$ = 68 mM, $[K^+]$ = 13.4 mM, $[Cl^-]$ = 102 mM, $[Ca^{2+}]$ = 0.6 mM, [bile] = 0.2 mM, protein (e.g., pepsin) concentration = 1.8 $g \cdot L^{-1}$ proteins, osmolality = 191 mOsm kg^{-1}, and ionic strength (I) = 0.1 M (Lindahl et al., 1997). Bile is composed of bile salts and acids, cholesterol and electrolytes. The fasted duodenum, the uppermost portion of the small intestine involved in digestion, has an average pH of 6.2, osmolality of 178 mOsm kg^{-1}, [bile salts] = 2.6 mM and total protein content of 3.1 g L^{-1} which includes proteins secreted from the stomach, pancreas and bile duct (e.g. trypsin, chymotrypsin, amylase, nucleases) (Kalantzi et al., 2006).

The objective of this study was to develop a biologically relevant *in vitro* assay to rapidly assess the biodurability of engineered nanomaterials in the human gastrointestinal tract. To

achieve this goal, we adapted an *in vitro* assay previously employed to examine the bioaccessibility of metals (Marschner et al., 2006; Oomen et al., 2003; Hamel et al., 1999; Plumlee et al., 2003) and organic contaminants in soil (Hack and Selenka, 1996). Alterations to reaction volumes and filtering processes allowed us to examine changes in physical properties of the nanoparticles, as well as the release of metals, effectively extending the use of the assay to engineered nanomaterials. The assay was designed to closely mimic the environment of the human stomach and duodenum in composition, residence time, pH and temperature. Previous studies have shown that the gastric phase of similar physiologically based extraction tests correlate well with *in vivo* rat and swine bioaccessibility data (Ruby et al., 1999; Pu et al., 2004). To demonstrate the functionality of this assay we employed semiconductor nanocrystals, or quantum dots (QDs) because of their convenient optical properties. The optical properties of QDs allow easy visualization, quantification and characterization. Semiconductor QDs typically consist of II–VI, III–V or IV–VI compound nanocrystals (e.g. CdSe, CdS, CdTe, InAs, GaN). The nanocrystalline core is often encased by a shell such as ZnS (Murphy and Coffer, 2002) and the quantum dot exterior is typically functionalized with organic molecules to improve biocompatibility or dispersibility (Medintz et al., 2005). The size-dependent properties of QDs make them attractive for use in optical devices, electronics and biological imaging (Murphy and Coffer, 2002; Parak et al., 2003; Hardman, 2006; Alivisatos, 1996; Alivisatos, 2004; Fu et al., 2005). Given the number of proposed applications, QDs are not only a convenient model system, but also have a growing potential as an environmental contaminant (Zhang et al., 2008). We aim to address the effects of pH, ligand chain length and proteins on the biodurability of PEGylated QDs under simulated gastrointestinal conditions.

Materials and methods

Chemicals

We obtained $CaCl_2$ (99.99%), NaCl (99.999%) KCl (Fluka, TraceSelect), KH_2PO_4 (99.99%), cadmium oxide (99.5%), trioctylphosphine oxide (TOPO, technical grade, 90%), trioctylphosphine (TOP, technical grade, 90%), zinc stearate (technical grade), sulfur powder (99.98%), selenium powder (100 mesh, >99.5%), tetramethylammonium hydroxide solution (TMAH, ~2.2 M) in methanol, pepsin (porcine stomach), mucin (Type III, porcine stomach), and pancreatin (porcine pancreas) from Sigma-Aldrich (St Louis, MO). We procured $MgCl_2 \cdot 6H_2O$ (puratronic) and $NaHCO_3$ (puratronic) from Alfa Aesar (Ward Hill, MA). Trace metal grade HCl and urea were purchased from Fisher Scientific (Chicago, IL). Bile salts were obtained from Oxoid LTD (England). Methoxy-terminated mercapto-poly(ethylene glycol) with a molecular mass of 350 Da (mPEG-thiol, PEG_{350}) was purchased from Diagnostic Chemicals Limited (Charlottetown, PE, Canada). Methoxy-terminated mercapto-poly(ethylene glycol) with a molecular mass of 5000 Dalton (PEG_{5000}) was purchased from RAPP Polymere (Tübingen, Germany).

Synthesis and functionalization of $CdSe_{core}/ZnS_{shell}$ quantum dots

We prepared $CdSe_{core}/ZnS_{shell}$ quantum dots from a CdO precursor using a modification of a published procedure (Huang et al., 2004; Metz et al., 2009). The quantum dots were

washed several times in either toluene or chloroform to remove excess organic materials remaining from the synthesis. The final product was stored in a slurry state.

The quantum dots were functionalized with mPEG-thiol of two molecular masses: 350 and 5000 Da. PEG ligands were used to replace the coordinating surface ligands used in synthesis (Aldana et al., 2005; Kang et al., 2004; Chan et al., 1998; Metz et al., 2009). Ligand exchange was performed in chloroform, driven by mass action. In a typical functionalization, a small amount of quantum dot slurry was suspended in chloroform, the QD number concentration was determined by UV-Visible (UV-Vis) spectroscopy, and a minimum of a 100-fold molar excess of the mPEG-thiol was added to the solution (Yu et al., 2003). Solution pH was adjusted to ≥12 by adding 4–5 drops of tetramethylammonium hydroxide (TMAH) in methanol (Aldana et al., 2005). The solution was shaken at 150 rpm at 42°C for 3 days on an incubating shaker, after which time excess organic ligands were removed and the PEGylated quantum dots were phase-transferred into water.

Exposure to simulated digestive fluids

We exposed PEGylated $CdSe_{core}/ZnS_{shell}$ quantum dots to simulated gastrointestinal (GI) fluids tract using a modification of a published method (Marschner et al., 2006). The QDs were exposed to the gastric phase alone, intestinal phase alone, or both in succession with or without the addition of gastric proteins. The compositions of the simulated digestive fluids are given in Table I. The pH of the simulated gastric and intestinal fluids was adjusted to 2 and 7.5, respectively, achieved by addition of HCl or solid $NaHCO_3$. The concentration of O_2 (aq) at 37°C was determined using a dissolved oxygen probe. After addition of QDs, samples were incubated at 37°C in a shaking water bath under constant agitation (200 rev min^{-1}) for 2, 6 or 8 hours. The 2-hour time period corresponds to the gastric phase, 6 hours mimics the retention time of the intestine, and 8 hours corresponds to the residence time in the stomach and duodenum. When exposed to both phases, intestinal fluid was added to the gastric solution following the gastric phase, and pH was adjusted to 7.5 with $NaHCO_3$. After incubation, samples were filtered for ~120 min·mL^{-1} at ~5000*g* through Millipore Centricon centrifugal concentrators with a regenerated cellulose membrane (nominal molecular weight cutoff = 10 000 Da). According to the manufacturer, the pore diameter of these filters is ~2.8 nm. Previous measurements (Metz et al., 2009) have shown the diameters of PEG_{350}- and PEG_{5000}-QDs to be approximately 6 nm and 14 nm respectively. Therefore, we would not expect the QDs to pass through the filter unless severely degraded.

Quantum dot characterization

UV-visible spectroscopy—UV-visible absorption spectroscopy was used to estimate CdSe core size and to determine molar number concentration. The position and amplitude of the first exciton peak provide information on the CdSe core size and QD number concentration, respectively (Yu et al., 2003). The wavelength of the first exciton peak decreases with QD core diameter. The absorbance of the first exciton peak is directly proportional to the number concentration of QDs in suspension. UV-visible spectra were collected with a Shimadzu PC-2401 UV-Visible spectrophotometer.

X-ray Photoelectron spectroscopy (XPS)—We employed XPS to verify the presence of the ZnS shell on the encasing the CdSe cores. A thin QD film was prepared by drying toluene or chloroform suspension of QDs onto a Si substrate. Spectra were collected under ultrahigh vacuum ($P < 4 \times 10^{-10}$ Torr) using a monochromatic Al K_α source (1486.6 eV) and a hemispherical analyzer with a multichannel detector (resolution 0.1–0.2 eV). The intensity in the Zn $2p_{3/2}$ region near 1022 eV binding energy demonstrated the presence of Zn in core-shell QDs samples. Control samples ($CdSe_{core}$-only QDs) lacked any peak in the region.

Attenuated total reflectance-Fourier transform infrared (ATR-FTIR) spectroscopy—We employed ATR-FTIR to assess the degree of surface functionalization of the QDs before and after exposure to simulated digestive fluids. Samples were filtered prior to analysis, and spectra of the filtrate and retentate were obtained. Infrared specta were acquired on a Digilab FTS 7000 with 500 co-added scans at 4 cm^{-1} resolution using a deuterated triglycine sulfate DTGS detector, or a Bruker Vertex 70 with 500 co-added scans at 4 cm^{-1} resolution using a mercury cadmium telluride MCT detector, and a 3-bounce diamond attenuated total internal reflection ATR element (MIRacle, Pike Technologies, Madison, WI).

Dynamic light scattering (DLS) was used to examine changes in hydrodynamic size of PEGylated QDs following exposure to simulated gastric fluids. Measurements were performed on a Malvern Zetasizer Nano-ZS and number-weighted values were reported. The derivation of number distributions from DLS data involves numerous assumptions; the hydrodynamic diameters reported in this paper should therefore not be regarded as absolute sizes. They are nonetheless useful for making comparisons among treatments. Each sample was measured in triplicate, with each measurement reporting the average of 10 runs.

Inductively coupled plasma-optical emission spectroscopy (ICP-OES)—Following exposure to the simulated digestive fluids and filtering, the filtrate and retentate were diluted to 10 mL with distilled deionized water (ddH_2O, 18 MΩ-cm resistivity, Barnstead NANOpure Ultrapure Water System, Dubuque, IA), and the pH was adjusted to < 2 with nitric acid for ICP-OES analysis. Quantum dot degradation was assessed by the amount of Cd and Zn in the filtrate compared to the retentate. Concentrations of each metal were calculated from peak intensities at three wavelengths (214.439 nm, 226.502 nm and 228.802 nm for Cd; 202.548 nm, 206.200 nm and 213.857 nm for Zn) using a Varian Vista-MPX ICP-OES with an axial-configured torch alignment. Measurements were taken in triplicate, and results at each wavelength were averaged. We note mass balances for Cd and Zn were incomplete due to loss to the filter. Filtering solutions of $CdCl_2$ demonstrated a ~30% loss of Cd^{2+} to the filter. Similar losses were shown for Zn^{2+} from $ZnCl_2$ solutions.

Viscosity measurements of mucin solutions were obtained using a Schott AVS 360 capillary viscometer. Measurements were taken at 37°C using a 0c capillary. Run times were averaged over 5 runs and dynamic v iscosity (η) was calculated.

Quartz crystal microbalance with dissipation (QCM-D; Q-Sense, Göteborg, Sweden) was employed to measure the adhesion of PEGylated quantum dots to a layer of mucin deposited

on gold-coated AT-cut quartz crystals with a fundamental frequency of 4.95 MHz (QSX-301, Q-Sense). Measurement of resonant frequency shift (Δ*f*, corresponding to changes in deposited wet mass) and the energy dissipation factor (Δ*D*, related to adlayer viscoelasticity) by QCM-D are detailed elsewhere (Rodahl et al., 1995; Rodahl and Kasemo, 1996). Prior to use, the crystals were cleaned by 10-min UV-ozone treatment (UV/Ozone ProCleaner, BioForce Nanotechnologies, Ames, IA) followed by 10-min immersion in a 1:1:5 solution of 30% H_2O_2: 25% NH_3: H_2O at 70°C, a dd$H_2$0 rinse, gentle drying under a stream of Ar, and a final 10-min UV-ozone treatment. Experiments were conducted at 37.0 ± 0.05 °C and at a constant 0.11-mL·min^{-1} liquid flowrate using a peristaltic pump (Ismatec Reglo, Glattbrugg, Switzerland). Prior to depositing the mucin layer, a 30 mM NaCl, pH 4 solution ("background solution") was pumped through the flow cell containing the crystal to allow *f* and *D* readings to stabilize. Experiments were commenced after obtaining stable *f* and *D* readings; Δ*f* and Δ*D* are reported relative to this initial condition. Procine mucin (25 mg·L^{-1}) in background solution was introduced into the cell, and mucin was allowed to deposit on the crystal surface for 30 min after which the flow was switched back to protein-free background solution to remove any unbound or loosely bound mucin. After this rinse, the analyte of interest (e.g., QD suspensions, methoxy-terminated PEG_{350}- or PEG_{5000}-thiol, or methoxy-terminated PEG_{300}- or PEG_{6000}-hydroxyl) was introduced to the flow chamber until both Δ*f* and Δ*D* stabilized. Finally, any unbound QDs or PEG molecules were removed by rinsing with background solution for ~5 min. Changes in resonant frequency and energy dissipation were measured up to the 13th harmonic. QCM-D data were modeled using QTools 3 (Q-Sense, Göteborg, Sweden) by applying a Voigt viscoelastic model to the Δ*f* and Δ*D* data to estimate shear modulus, dynamic viscosity and adlayer thickness (Voinova et al., 1999). Model inputs were liquid phase density (1001 kg·m^{-3}), measured liquid phase viscosity (7.1×10^{-4} Pa·s), and attached layer density (1450 kg·m^{-3} taken from the literature for "high-density" mucin layers, Nordman et al., 1998).

Results

Quantum dot characterization

We employed ultraviolet-visible absorption, x-ray photoelectron (XPS) and Fourier transform infrared (FTIR) spectroscopies to characterize the PEG-coated QDs. The UV-Vis absorption spectra of the QDs exhibited steadily increasing absorbance as wavelength declined, a strong absorbance peak centered at 525 nm corresponding to the first exciton of the CdSe core, followed by a near linear increase in absorbance as wavelength decreased beyond the first exciton peak (Figure 1a). Based on the first exciton peak position, the size of the unaltered CdSe core is estimated to be 2.6 ± 0.1 nm (Yu et al., 2003; Peng et al., 1998). The use of UV-Vis absorption spectroscopy to determine the absolute size of QD cores has recently been questioned (Yu et al., 2007); however, the approach remains useful for comparing QD core size among treatments (*vide infra*). X-ray photoelectron spectroscopy demonstrated that the thickness of the ZnS shell did not exceed 1 nm (data not shown). FTIR spectra of PEGylated QDs exhibited at least eight identifiable peaks (Figure 1b), all attributable to poly(ethylene glycol) based on previous characterization of PEG monolayers on gold surfaces (Harder et al., 1998; Valiokas et al., 1999; Valiokas et al., 2001). Peak assignments are given in Table II. The FTIR data are consistent with complete

exchange of PEG-thiol for the coordinating ligand used in QD synthesis. The lengths of the fully extended PEG ligands were estimated to be 1 nm and 4.5 nm for PEG_{350} and PEG_{5000} (Parak et al., 2005). Therefore, the approximate diameter of PEG_{350}-coated QDs was 6 nm, while that of the PEG_{5000}-coated QDs was near 14 nm.

Transformation of PEG_{350}-coated QDs upon exposure to simulated digestive fluids

Effects on core size and number concentration of quantum dots in suspension—We exposed PEG_{350}-QDs to simulated gastric fluid, intestinal fluid or both in succession (GI) and used UV-Vis spectroscopy to evaluate changes in QD core size and number concentration (Figure 2a). Initial exposures of PEG_{350}-QDs to simulated digestive fluids were conducted in the absence of gastric proteins. Gastric fluid exposure resulted in a loss of the first exciton peak and very low absorbance (~0.002 at 450 nm). The position of the first exciton peak was not discernibly altered upon exposure to the intestinal and GI fluids, indicating that these biological fluids did not affect QD core size. The magnitude of the first exciton peak for PEG_{350}-QDs decreased after exposure to intestinal and GI fluids, corresponding to 20% and 45% declines in QD concentration following intestinal and GI fluid exposures.

Effects on ligand attachment—The PEG-thiol ligand was lost from the QDs during exposure to the gastric fluid, as confirmed by FTIR spectroscopy. After exposure to the simulated gastric fluid, nearly all the PEG_{350} ligand appeared in the filtrate indicating that the majority was no longer associated with the QDs (Figure 2b). Removal of surface ligand from QDs exposed to intestinal or GI conditions was much less pronounced (data not shown).

Release of metals—We assessed the extent of QD dissolution during exposure to the simulated digestive fluids by separating the PEG_{350}-QDs from suspension as described above and analyzing the filtrate and retentate for Cd and Zn by ICP-OES. Zinc was present in the filtrate from untreated QDs (pH $\simeq$ 4.5, $I \leq 0.05$ mM) and after all exposures (Figure 2c). With the exception of the gastric fluid-exposed QDs, the majority of the zinc was present in the retentate (i.e. associated with the QDs) (Figure 2c).

Cadmium was released from the PEG_{350}-QDs upon exposure to the simulated gastric fluid, but apparently not in the intestinal phase (Figure 2d). The filtrate of the gastric fluid-exposed QDs contained ~10% of the total recovered cadmium; no Cd was detected in the filtrates of unexposed QD suspensions, QD suspensions exposed to intestinal fluid or sequentially to gastric and intestinal fluids. Lack of Cd in the filtrates of GI fluid exposed QDs is possibly due to the formation of precipitates on the filter.

Effect of ligand chain length on QD biodurability in simulated digestive fluids

Exposure of PEG_{5000}-coated QDs to simulated gastric conditions resulted in complete loss of the first exciton peak (Figure 3a). In contrast to the extremely low absorbance observed when PEG_{350}-QDs were exposed to similar conditions (Figure 2a), gastric fluid-exposed PEG_{5000}-QD suspension exhibited relatively high absorbance, increasing monotonically as wavelength shortened.

Exposure of PEG_{5000}-QDs to simulated intestinal conditions had little impact on their UV-visible absorption spectrum (Figure 3a). The UV-visible spectrum of the PEG_{5000}-QD sequentially exposed to gastric and intestinal fluids displayed a first exciton peak of much smaller amplitude than that of the unexposed quantum dots (Figure 3a). Number-averaged hydrodynamic diameters for untreated and gastric phase-exposed PEG_{5000}-QDs were 33 ± 5 nm and 68 ± 15 nm.

We assessed the release of cadmium and zinc from the PEG_{5000}-QDs by ICP-OES as described above. Only the gastric fluid exposure resulted in measurable Cd and Zn in the filtrate (Figure 3b and c).

Effect of changing gastric pH on quantum dot biodurability

The pH of gastric fluid *in vivo* generally ranges between pH 1 and 6 (Kalantzi et al., 2006; Lindahl et al., 1997). We therefore examined biodurability of PEGylated QDs at pH 4 and pH 6. For PEG_{350}-QDs, the first exciton peak remained in the UV-Vis spectra at both pH values, and QD concentration declined by a small amount (12.3%). PEG_{5000}-QDs appeared mostly intact at pH 6, with a concentration loss similar to that following intestinal fluid exposure. Following 2-h exposure to the pH 4 gastric solution, UV-Vis spectra of PEG_{5000}-QDs exhibited a low amplitude, broad exciton peak. suggesting breakdown of the QDs. The diminished first exciton peak was likely due to aggregation/agglomeration of the PEG_{5000}-QDs due to the ionic strength of the pH 4 solution (I = 0.07 M). Previous pseudo-steady state titrations of these nanoparticles under low ionic strength conditions demonstrated that suspensions were stable at pH ≥ 3.5(Metz et al., 2009). Furthermore, PEG_{5000}-QD suspensions were stable for at least 2 h at pH 4 in 0.03 M NaCl.

Influence of proteins on the gastric biodurability of quantum dots

The data presented above were obtained in exposures to simulated gastrointestinal fluids that lacked proteins. We subsequently examined the impact of gastric (viz. pepsin and mucin) and intestinal proteins (viz. pancreatin) on the biodurability of PEG_{350}- and PEG_{5000}-QDs. Pepsin is a 35-kDa digestive protease (Sepulveda et al., 1975). Mucin is a large (1- to 10-MDa), heavily glycosylated, multimeric protein (Bansil et al., 2005). Pancreatin is a mixture of pancreatic enzymes including amylase, lipase, proteases (e.g. trypsin) and nucleases.

Pepsin, mucin or both were added to the simulated gastric fluid, and UV-Vis spectra were acquired to examine the influence of these proteins on the gastric biodurability of QDs. Inclusion of pepsin in the gastric fluid did not appear to affect the degradation of PEG_{350}- or PEG_{5000}-QDs. The UV-Vis spectra (Figure 4) were identical to those obtained from gastric fluid exposures lacking protein for both types of QDs (Figures 2 and 3). The first exciton peak was diminished, but discernable in the UV-visible spectra of PEG_{350}- and PEG_{5000}-QDs exposed to mucin-containing gastric fluid (Figure 4) suggesting that the glycoprotein partially protected the QDs from degradation. Similar results were found for gastric solutions including mucin at pH 4 and 7 (data not shown). The inclusion of both proteins in the gastric phase yielded UV-Vis spectra identical to those obtained from the mucin treatment suggesting addition of pepsin failed to effect additional protection (data not

shown). Inclusion of the protein mixture pancreatin in simulated intestinal fluid resulted in no discernable effect on QD biodurability (data not shown).

Quantum dot diffusivity in the presence of mucin

We measured the dynamic viscosities of gastric solutions containing mucin and the diffusivities of PEG_{350}– and PEG_{5000}-QDs under simulated gastric conditions in the absence and presence of mucin. The measured dynamic viscosity of mucin-free and mucin-containing gastric solutions at 37°C were 0.71 and 0.99 cP. PEG_{350}- and PEG_{5000}-QDs exhibited diffusivities of 2.64×10^{-11} and 8.10×10^{-12} $m^2 \cdot s^{-1}$(corresponding to number-averaged hydrodynamic diameters of ~25 and ~78 nm) in mucin-free gastric fluid after 15-min contact time as determined by DLS. PEG_{350}- and PEG_{5000}-QDs number distributions in the presence and absence of mucin are shown in Figure 5. For both PEG_{350}- and PEG_{5000}-QDs, peak position shifts to larger sizes when mucin is present in the solution. Measurement of the same samples using the refractive index of mucin, rather than that of ZnS, resulted in disappearance of the QD peak when mucin was present in the solution (data not shown).

Quantum dot mucoadhesion

To further investigate the interaction of QDs with mucin we examined the adhesion of quantum dots to mucin layers deposited on gold-coated quartz crystals by QCM-D. These experiments were conducted at pH 4 in 0.03 M NaCl. The PEG_{5000}- and PEG_{350}-QD suspensions were stable under these solution conditions, consistent with previous pseudo-steady state titrations of these nanoparticles (Metz et al., 2009). As seen in Figure 6a and b, adsorption of mucin onto the surface of the QCM-D crystal occurred rapidly, as evidenced by the decline in resonance frequency and increase in dissipation upon introduction of the glycoprotein. No changes in f or D for the mucin adlayer were observed during rinsing with background solution. Introduction of PEG_{5000}-QDs to the liquid phase resulted in a decrease in f and increase in D indicating an increase in deposited mass and viscoelasticity. In contrast, addition of PEG_{350}-QDs produced declines in both f and D suggesting an increase in mass but a decrease in viscoelasticity (i.e. the layer became stiffer). The Δf and ΔD were smaller for the PEG_{350}-QDs than for those functionalized with PEG_{5000}. In both experiments, the changes in both f and D occurring upon subsequent rinsing were small relative to those produced by QD deposition.

Discussion

Transformation of PEGylated QDs upon exposure to simulated digestive fluids

Loss of the first exciton peak and diminished UV-visible absorbance of gastric fluid-exposed PEG_{350}-QDs (Figure 2a) is consistent with either dissolution of the CdSe core or aggregation/agglomeration of QDs followed by sedimentation. The presence and magnitude of the first exciton peak following sequential exposure to gastric and intestinal fluids (GI fluid exposure) indicates that ≥ 55% of the CdSe cores remained intact during gastric fluid exposure. Upon pH adjustment at the initiation of the intestinal phase, PEG ligands could reattach to the intact cores. Reattachment of PEG ligands could explain the reappearance of the exciton peak following GI fluid exposures of PEG_{350}-QDs. These data suggest that aggregation/agglomeration with subsequent sedimentation contributed to pronounced

decline in UV-Vis absorbance resulting from gastric fluid exposure. Aggregation/agglomeration of the PEG_{350}-QDs was confirmed by DLS (number-averaged hydrodynamic diameters were 10 ± 2 nm for untreated PEG_{350}-QDs and 459 ± 35 nm for gastric fluid-exposed QDs).

Aggregation/agglomeration of PEG_{350}-QDs following gastric fluid exposure can be rationalized considering the pH of the fluid and the pK_a of PEG-thiol. The PEG-thiol attachment to zinc in the QD shell is dynamic (i.e. a dynamic equilibrium exists between the ligands attached to the surface and those in solution (Ulman, 1996)). High proton activities (low pH) favor protonation of the thiol moiety in solution, decreasing the population of PEG-thiolate molecules available to bind to the Zn in the QD shell. Suspensions of similarly sized $CdSe_{core}/ZnS_{shell}$ quantum dots functionalized with a 3-mercapto-1-propanol and 3-mercaptopropionic acid via the thiol moiety (pK_a values between 9 and 10) were destabilized below pH 4 (Aldana et al., 2005). Removal of the PEG ligand would favor aggregation/agglomeration of the hydrophobic $CdSe_{core}/ZnS_{shell}$ QDs, destabilizing the suspension. Indeed, our data showed loss of PEG ligand from PEG_{350}-QDs following gastric fluid exposure and subsequent aggregation/agglomeration of the particles. Hydrodynamic diameters of PEG_{350}-QDs remaining in suspension after gastric fluid exposure at pH 4 (80 ± 12 nm) or 6 (80 ± 15 nm) indicated some aggregation/agglomeration relative to the quantum dots in ddH_2O (10 ± 2 nm). However, the aggregation/agglomeration was not as severe as for those exposed at pH 2. The aggregation/agglomeration at pH 4 and 6 is most likely attributable to the ionic strength of the gastric fluid. Pseudo-steady state titration of PEG_{350}-QDs demonstrated that the quantum dot suspension was stable at pH ≥ 3.5 at lower ionic strengths (Metz et al., 2009). These data are consonant with the idea of a destabilized suspension at pH 2 due to the loss PEG thiol ligands. Gastric fluid pH *in vivo* varies by individual, and is influenced by the presence and pH of ingested food (Kalantzi et al. 2006; Lindahl et. al., 1997). Examination of gastric biodurability of engineered nanoparticles at multiple pH values is therefore warranted.

The ZnS shell dissolved under the conditions used in these experiments with the most severe degradation occurring in the low pH gastric fluid. Erosion of the ZnS shell during the gastric phase would expose the CdSe core to an acidic environment and result in the release of $Cd^{II}(aq)$. The presence of a small percentage of the $Cd^{II}(aq)$ in the filtrate of PEG_{350}-QDs exposed to gastric fluid, but not to intestine or GI fluids, is consonant with this idea. Speciation calculations, including all ions present in the simulated gastric fluid, indicate that under simulated gastric conditions 94% of the total Cd released would be Cd^{2+}. Stability constants used in the calculations were obtained from Stumm and Morgan (1996) and Bard et al. (1985). The remaining 6% were predicted to be predominately $Cd_3(PO_4)_2{}^0$ (aq) (3.5 %) and $CdCl_2{}^0$ (aq) (1.6%). The small percentage of Cd released might be explained by the decreased surface area in contact with the acidic solution due to aggregation/agglomeration. The lack of Zn in the filtrate of GI exposed QDs could be due to complexation of Zn^{2+} by PEG-thiol preventing passage of Zn through the filter. To examine this possibility, we filtered solutions of $ZnCl_2$ and either PEG_{350}-thiol or PEG_{5000}-thiol following exposure to the simulated gastric, intestinal and GI fluids. All recoverable Zn^{2+} in the experiments

following gastric fluid exposure was in the filtrate; in contrast, following intestinal or GI fluid exposure approximately half of the recovered Zn^{2+} remained in the retentate.

Pourbaix (pε/pH) diagrams have been used to evaluate the bioaccessibility solid-phase metals in biological fluids (Plumlee et al., 2006). We therefore examined the extent to which our experimental data corresponded to predictions based on pε/pH calculations. The Pourbaix diagrams indicate that both ZnS and CdSe should be thermodynamically stable in the gastric (pH 2, pε −0.01) and intestinal (pH 7.5, pε 0.16) fluids (see Appendix). These predictions contrast with our observation of (partial) dissolution of both materials upon exposure to gastric fluid. We note that the Pourbaix diagrams were constructed for 25°C rather than 37°C because thermodynamic data for some species (e.g., Se^{2-}) was lacking. However, we expect this relatively small difference in temperature to have minimal effect on the diagram. More importantly, the diagrams were produced assuming equilibrium and not considering the presence of a gas phase or PEG-thiol ligands. In the gastric phase of the experimental system employed, the fluid-to-headspace ratio was 0.15. Volatilization of H_2S (pK_a = 6.89) and H_2Se (pK_a = 3.98) into the headspace would deplete sulfide species in solution and drive the dissolution of ZnS and CdSe. At equilibrium and 37°C, 70% of H_2S and 69% of H_2Se would be present in the headspace. In addition to the volatilization of H_2S and H_2Se, the presence of PEG-thiol ligands in solution may have also promoted dissolution (Ulman, 1996). Additional factors can limit application of Pourbaix diagrams for predicting the speciation of nanoscale metal oxides and chalcogenides at present. Pourbaix diagrams are usually constructed using reduction potentials and solubility products of bulk phase materials. However, reduction potentials of metal oxides and chalcogenides decrease as the quantum confinement regime is reached (Rossetti et al., 1983; Hoyer and Weller, 1994), indicating oxidation of these materials occurs more readily than for the bulk materials. Solubility products for nanoparticles are higher than for their bulk counterparts (Stumm and Morgan, 1996). Furthermore, the most thermodynamically stable polymorph of a mineral can change with particle size (Chernyshova et al., 2007).

Effect of ligand chain length—Extending the poly(ethylene glycol) chain-length prolongs the circulation of particles and/or drugs within the body, a feature attractive for drug delivery systems (Harris et al., 2001). Previous studies have shown that CdSe nanocrystals with shorter ligands are more susceptible to degradation (Aldana et al., 2001; Metz et al., 2009), but the extent of degradation also depends significantly on the overall chemical composition of the solution. Our results showed that PEG_{5000}-QDs were severely degraded during gastric fluid exposure, but appeared largely intact following intestinal fluid exposure. Low absorbance and the broadness of the first exciton peak following GI fluid exposure of PEG_{5000}-QDs limits our interpretation of these results. The broadness of the peak, however, may indicate a large distribution of CdSe core sizes. The PEG_{5000} ligand likely provided superior suspension stability increasing the effective exposure time of PEG_{5000}-QDs during the gastric phase and increasing the degree of degradation. The longer PEG_{5000} particles were likely better able to encapsulate the particle in a complete polymer shell; consequently, detachment of the thiol group may have had less effect on the overall stability of the nanoparticles. Destabilization of the PEG_{350}-QD suspension during gastric fluid exposure appeared to partially protect the quantum dots from degradation.

Aggregation/agglomeration would reduce the QD surface area exposed to the low pH solution.

Influence of proteins on gastric biodurability of QDs

Initial experiments were conducted in the absence of proteins to allow us to (1) evaluate the importance of including proteins in the simulated digestive fluids (many gastrointestinal assays exclude proteins) and (2) delineate some of the processes likely to govern the gastrointestinal biodurability of QDs. However, actual digestive fluids are more complex than the solution of electrolytes, urea and bile salts used. In particular, interactions between nanoparticles and proteins are expected to influence their biodurability. Nanoparticle-protein interactions have been shown to influence the rate of cellular uptake as well as subcellular localization (Maysinger, 2007; Patil et al., 2007; Lynch et al., 2007).

The DLS data suggest that hindered diffusion was not the main mechanism by which mucin protected QDs from decomposition in the gastric phase. This effect would be manifested by diminished diffusivity in the mucin-containing gastric solution relative to gastric solution without added mucin. Using the measured viscosity of the mucin-containing gastric solution and the QD diameters determined in the absence of mucin, we used the Stokes-Einstein equation to calculate diffusivities of 1.91×10^{-11} and 5.87×10^{-12} $m^2 \cdot s^{-1}$ for PEG_{350}- and PEG_{5000}-QDs, respectively, in mucin-containing gastric fluid. These calculated values are only slightly smaller than those for PEG_{350}- and PEG_{5000}-QDs measured in the absence of mucin (2.64×10^{-11} and 8.10×10^{-12} $m^2 \cdot s^{-1}$). In contrast, the diffusivities for PEG_{350}- and PEG_{5000}-QDs measured in mucin-containing gastric fluid were much smaller (3.42×10^{-12} and 2.67×10^{-12} $m^2 \cdot s^{-1}$). Drawing definitive conclusions from these results is difficult because the difference in size between the QDs and mucin is large; however, these data suggest that the interaction of the QDs with mucin is not solely due to the larger viscosity of the mucin-containing solution.

The protective action of mucin may instead arise from absorption of QDs into the mucin matrix. In the matrix, the QDs would be shielded from the aqueous environment that would otherwise degrade the nanoparticles. Mucin forms a protective barrier against self-digestion of stomach epithelial cells by aggregating and forming a gel at pH 2 (Hong et al., 2005; Celli et al., 2005). Quantum dot association with the mucin gel matrix would protect the PEG_{5000}-QDs from the acid-induced degradation observed in the simulated gastric fluid in the absence of proteins. QCM-D data support such an association between the PEGylated QDs and the mucin matrix. Voigt viscoelastic modeling of the QCM-D data indicated that the mucin generally formed a stable 7–10 nm thick layer on the gold sensor surface. The increase in attached mass (decrease in f) upon QD introduction suggests that a fraction of both types of QDs adhered to or entered into the mucin layer. Quantum dot association with the mucin layer increased the calculated thickness of the attached layer by ~3 nm for PEG_{5000}-QDs and ~0.2 nm for PEG_{350}-QDs). Dissipation increased upon introduction of PEG_{5000}-QDs, corresponding to an increase in adlayer viscoelasticity. Conversely, addition of PEG_{350}-QDs produced a decrease in D, corresponding to a decrease in viscoelasticity and suggesting the PEG_{350}-QDs integrated more fully into the mucin layer, stiffening the adlayer. The PEG_{350}- and PEG_{5000}-QD suspensions were stable under the conditions

employed in the QCM-D experiments, consistent with the pseudo-steady state titrations mentioned above. The similar changes in *f* and *D* cannot therefore be explained by binding of PEG_{5000}-thiol released from the QDs.

Association with mucin may have implications for the uptake on nanoparticles within the GI tract. Entrapment of nanoparticles within the mucus layer during their transit through the GI tract and subsequent excretion through natural turnover processes may limit the potential for uptake (Ponchel and Irache, 1998). However, if NPs are able to diffuse through the mucus layer, interactions with cell surfaces, and the potential for uptake/translocation, may occur (Florence and Hussain, 2001). Our results indicate that future assessment of gastrointestinal biodurability and uptake of engineered NP should explicitly consider the role of mucin.

The assay developed here can be used to evaluate the gastrointestinal biodurablity of a wide variety of nanoparticles and can be coupled to *in vitro* systems to assess nanoparticle uptake by and toxicity to intestinal epithelia. The assay could be used to advantage in assessing nanoparticles as drug delivery systems and in prioritizing nanomaterials for further *in vivo* investigation. The *in vitro* system presented here was modeled after the human gastrointestinal tract. The extension of this approach to other species should be straightforward provided digestive fluid composition has been determined.

Acknowledgments

This work was supported by the National Science Foundation award DMR-0425880. We thank Jackie Bastyr-Cooper for ICP-OES analysis, and Paul F. Nealy and Mikhail Efremov for instrumental access and assistance, and Nita Sahai for use of data analysis using the geochemist's workbench software. K.H.J. was supported by a NIH Training Grant (NIH 5 T32 GM08349).

References

Aldana J, Lavelle N, Wang YJ, Peng XG. Size-dependent dissociation pH of thiolate ligands from cadmium chalcogenide nanocrystals. J Am Chem Soc. 2005; 127:2496–2504. [PubMed: 15725004]

Aldana J, Wang YA, Peng XG. Photochemical instability of CdSe nanocrystals coated by hydrophilic thiols. J Am Chem Soc. 2001; 123:8844–8850. [PubMed: 11535092]

Alivisatos AP. Semiconductor clusters, nanocrystals, and quantum dots. Science. 1996; 271:933–937.

Alivisatos P. The use of nanocrystals in biological detection. Nature Biotechnol. 2004; 22:47–52. [PubMed: 14704706]

Bansil R, Stanley E, LaMont JT. Mucin biophysics. Annu Rev Physiol. 2005; 57:635–657. [PubMed: 7778881]

Bard, AJ.; Parson, R.; Jordan, J. Standard potentials in aqueous solution. Marcus Dekker; New York: 1985.

Boldt K, Bruns OT, Gaponik N, Eychmuller A. Comparative examination of the stability of semiconductor quantum dots in various biochemical buffers. J Phys Chem B. 2006; 110:1959–1963. [PubMed: 16471768]

Borm PJA, Robbins D, Haubold S, Kuhlbusch K, Fissan H, Donaldson K, Schins R, Stone V, Kreyling W, Lademann J, Krutmann J, Warheit D, Oberdörster E. The potential risks of nanomaterials: A review carried out for ECETOC. Particle and Fibre Toxicol. 2006; 3

Celli J, Gregor B, Turner B, Afdhal NH, Bansil R, Erramilli S. Viscoelastic properties and dynamics of porcine gastric mucin. Biomacromolecules. 2005; 6:1329–1333. [PubMed: 15877349]

Center for Science, Technology and Public Policy Workshop. The nanotechnolocy-biology interface: exploring models for oversight. University of Minnesota; 2006.

Chan WCW, Nie SM. Quantum dot bioconjugates for ultrasensitive nonisotopic detection. Science. 1998; 281:2016–2018. [PubMed: 9748158]

Chernyshova IV, Hochella MF, Madden AS. Size-dependent structural transformations of hematite nanoparticles. 1 Phase transition. Phys Chem Chem Phys. 2007; 9:1736–1750. [PubMed: 17396185]

Dunphy KA, Guzmán D, Taylor MR, Banfield JF. Environmental risks of nanotechnology: National Nanotechnology Initiative funding, 2000–2004. Environ Sci Technol. 2006; 40:1401–1407. [PubMed: 16568748]

Florence AT, Hussain N. Transcytosis of nanoparticle and dendrimer delivery systems: Evolving vistas. Adv Drug Del Rev. 2001; 50:S69–S89.

Fu A, Gu W, Larabell C, Alivisatos AP. Semiconductor nanocrystals for biological imaging. Curr Opin Neurobiol. 2005; 15:568–575. [PubMed: 16150591]

Hack A, Selenka F. Mobilization of PAH and PCB from contaminated soil using a digestive tract model. Toxicol Lett. 1996; 88:199–210. [PubMed: 8920737]

Hamel SC, Ellickson KM, Lioy PJ. The estimation of bioaccessibility of heavy metals in soils using artificial biofluids by two novel methods: mass-balance and soil recapture. Sci Total Environ. 1999; 244:273–283. [PubMed: 10635599]

Hankare P, Chate P, Asabe M, Delekar S, Mula I, Garadkar K. Characterization of $Cd_{1-x}Zn_xSe$ thin films deposited at low temperature by chemical route. J Mater Sci-Mater Electron. 2006; 17:1055–1063.

Harder P, Grunze M, Dahint R, Whitesides GM, Laibinis PE. Molecular conformation in oligo(ethylene glycol)-terminated self-assembled monolayers on gold and silver surfaces determines their ability to resist protein adsorption. J Phys Chem B. 1998; 102:426–436.

Hardman R. A toxicologic review of quantum dots: Toxicity depends on physicochemical and environmental factors. Environ Health Perspect. 2006; 114:165–172. [PubMed: 16451849]

Harris JM, Martin NE, Modi M. PEGylation - A novel process for modifying pharmacokinetics. Clin Pharmacokinet. 2001; 40:539–551. [PubMed: 11510630]

Hong Z, Chasan B, Bansil R, Turner BS, Bhaskar KR, Afdhal NH. Atomic force microscopy reveals aggregation of gastric mucin at low pH. Biomacromolecules. 2005; 6:3458–3466. [PubMed: 16283779]

Hoyer P, Weller H. Size-dependent redox potentials of quantized zinc-oxide measured with an optically transparent thin-layer electrode. Chem Phys Lett. 1994; 221:379–384.

Huang GW, Chen CY, Wu KC, Ahmed MO, Chou PT. One-pot synthesis and characterization of high-quality CdSe/ZnX (X = S, Se) nanocrystals via the CdO precursor. J Cryst Growth. 2004; 265:250–259.

ICF international. Characterizing the Environmental, Health and Safety Implications of Nanotechnology: Where Should the Government go from here?. Fairfax, VA: 2006.

Kalantzi L, Goumas K, Kalioras V, Abrahamsson B, Dressman JB, Reppas C. Characterization of the human upper gastrointestinal contents under conditions simulating bioavailability/bioequivalence studies. Pharm Res. 2006; 23:165–176. [PubMed: 16308672]

Kale RB, Lokhande CD. Band gap shift, structural characterization and phase transformation of CdSe thin films from nanocrystalline cubic to nanorod hexagonal on air annealing. Semicond Sci Technol. 2005; 20:1–9.

Kang EC, Ogura A, Kataoka K, Nagasaki Y. Preparation of water-soluble PEGylated semiconductor nanocrystals. Chem Lett. 2004; 33:840–841.

Lindahl A, Ungell AL, Knutson L, Lennernäs H. Characterization of fluids from the stomach and proximal jejunum in men and women. Pharm Res. 1997; 14:497–502. [PubMed: 9144738]

Lynch I, Cedaevall T, Lundqvist M, Cabaleiro-Lago C, Linse S, Dawson KA. The nanoparticle-protein complex as a biological entity; a complex fluids and surface science challenge for the 21st century. Adv Colloid Interface Sci. 2007; 134–135:167–174.

Marschner B, Welge P, Hack A, Wittsiepe J, Wilhelm M. Comparison of soil Pb in vitro bioaccessibility with Pb pools from a sequential soil extraction. Environ Sci Technol. 2006; 40:2812–2818. [PubMed: 16683628]

Maxim LD, Hadley JG, Potter RM, Niebo R. The role of fiber durability/biopersistance of silica-based synthetic vitreous fibers and their influence on toxicology. Regul Toxicol Pharmacol. 2006; 46:42–62. [PubMed: 16837114]

Maysinger D. Nanoparticles and cells: Good companions or doomed partnerships. Org Biomol Chem. 2007; 5:2335–2342. [PubMed: 17637950]

Medintz IL, Uyeda HT, Goldman ER, Mattoussi H. Quantum dot bioconjugates for imaging, labeling and sensing. Nat Mat. 2005; 4:435–446.

Metz KM, Mangham AN, Bierman MJ, Song J, Hamers RJ, Pedersen JA. Engineered nanomaterial transformation under oxidative environmental conditions: Development of an in vitro biomimetic assay. Environ Sci Technol. 2009 in press.

Muhle H, Bellmann B. Significance of the biodurability of man-made vitreous fibers to risk assessment. Environ Health Perspect. 1997; 105:1045–1047. [PubMed: 9400698]

Murphy CJ, Coffer JL. Quantum Dots: A Primer. Appl Spectrosc. 2002; 56:16A–26A.

Nanotechnology white paper. United States Environmental Protection Agency; Washington, DC: 2007.

National Nanotechnology Initiative. Environmental, Health and Safety Research Needs for Engineered Nanoscale Materials. National Science and Technology Council; Washington, DC: 2006.

Nel A, Xia T, Mädler L, Li N. Toxic potential of materials at the nanolevel. Science. 2006; 311:622–627. [PubMed: 16456071]

Nordman H, Davies JR, Carlstedt I. Mucus glycoproteins from pig gastric mucosa: different mucins by the surface epithelium and the glands. Biochem J. 331:687–694. [PubMed: 9560293]

Oomen AG, Rompelberg CJM, Bruil MA, Dobbe CJG, Pereboom DPKH, Sips AJAM. Development of an in vitro digestion model for estimating the bioacceccibility of soil contaminants. Arch Environ Contam Toxicol. 2003; 44:281–287. [PubMed: 12712286]

Parak WJ, Pellegrino T, Plank C. Labeling of cells with quantum dots. Nanotechnology. 2005; 16:R9–R25. [PubMed: 21727419]

Parak WJ, Gerion D, Pellegrino T, Zanchet D, Micheel C, Williams SC, Boudreau R, Le Gros MA, Larabell CA, Alivisatos AP. Biological applications of colloidal nanocrystals. Nanotechnol. 2003; 14:R15–R27.

Patil S, Sandberg A, Heckert E, Self W, Seal S. Protein adsorption and cellular uptake of cerium oxide nanoparticles as a function of zeta potential. Biomaterials. 2007; 28:4600–4607. [PubMed: 17675227]

Peng XG, Wickham J, Alivisatos AP. Kinetics of II-VI and III-V colloidal semiconductor nanocrystal growth: “focusing” of size distributions. J Am Chem Soc. 1998; 120:5343–5344.

Plumlee, GS.; Morman, SA.; Ziegler, TL. The toxicological geochemistry of earth materials: An overview of processes and the interdisciplinary methods used to understand them. In: Sahai, N.; Schoonen, MAA., editors. Reviews in Mineralogy and Geochemistry: Medical Mineralogy and Geochemistry. Geochemical Society and Mineralogical Society of America; Chantilly, VA: 2006. p. 5-57.

Ponchel G, Irache JM. Specific and non-specific bioadhesive particulates for oral delivery. Adv Drug Del Rev. 1998; 34:191–219.

Pu X, Lee LS, Galinsky RE, Carlson GP. Evaluation of a rat model versus a physiologically based extraction test for assessing phenanthrene bioavailability from soils. Toxicol Sci 2004. 79:10–17.

Rodahl M, Höök F, Krozer A, Brzezinski P, Kasemo B. Quartz crystal microbalance setup for frequency and Q-factor measurements in gaseous and liquid environments. Rev Sci Instrum. 1995; 66:3924–3930.

Rodahl M, Kasemo B. A simple setup to simultaneously measure the resonant frequency and the absolute dissipation factor of a quartz crystal microbalance. Rev Sci Instrum. 1996; 67:3238–3241.

Rossetti R, Nakahara S, Brus LE. Quantum size effects in the redox potentials, resonance raman spectra, and electronic spectra of CdS crystallites in aqueous solution. J Chem Phys. 1983; 79:1086–1087.

Ruby MV, Schoof R, Brattin W, Goldade M, Post G, Harnois M, Mosby DE, Casteel SW, Berti W, Carpenter M, Edwards D, Cragin D, Chappell W. Advances in Evaluating the Oral Bioavailability

of Inorganics in Soil for Use in Human Health Risk Assessment. Environ Sci Technol. 1999; 33:3697–3705.

Sepulveda P, Marciniszyn J, Liu D, Tang J. Primary structure of porcine pepsin. J Biol Chem. 1975; 250:5082–5088. [PubMed: 1097438]

Smith AM, Duan H, Rhyner MN, Ruan G, Nie S. A systematic examination of surface coatings on the optical and chemical properties of semiconductor quantum dots. Phys Chem Chem Phys. 2006; 8:3895–3903. [PubMed: 19817050]

Sperling RA, Liedl T, Duhr S, Kudera S, Zanella M, Lin CAJ, Chang WH, Braun D, Parak WJ. Size determination of (bio)conjugated water-soluble colloidal nanoparticles: A comparison of different techniques. J Phys Chem C. 2007; 111:11552–11559.

Stumm, W.; Morgan, JJ. Aquatic Chemistry. 3. John Wiley and Sons; New York: 1996.

Ulman A. Formation and structure of self-assembled monolayers. Chem Rev. 1996; 96:1533–1554. [PubMed: 11848802]

Valiokas R, Svedhem S, Ostblom M, Svensson SCT, Liedberg B. Influence of specific intermolecular interactions on the self-assembly and phase behavior of oligo(ethylene glycol)-terminated alkanethiolates on gold. J Phys Chem B. 2001; 105:5459–5469.

Valiokas R, Svedhem S, Svensson SCT, Liedberg B. Self-assembled, monolayers of oligo(ethylene glycol)-terminated and amide group containing alkanethiolates on gold. Langmuir. 1999; 15:3390–3394.

Voinova MV, Rodahl M, Jonson M, Kasemo B. Viscoelastic acoustic response to layered polymer films at fluid-solid interfaces: continuum mechanics approach. Physica Scripta. 1999; 59:391–396.

Yu WW, Chang E, Falkner JC, Zhang JY, Al-Somali AM, Sayes CM, Johns J, Drezek R, Colvin VL. Forming biocompatible and nonaggregated nanocrystals in water using amphiphilic polymers. J Am Chem Soc. 2007; 129:2871–2879. [PubMed: 17309256]

Yu WW, Qu LH, Guo WZ, Peng XG. Experimental determination of the extinction coefficient of CdTe, CdSe, and CdS nanocrystals. Chem Mat. 2003; 15:2854–2860.

Zhang Y, Chen Y, Westerhoff P, Crittenden JC. Stability and removal of soluble CdTe quantum dots in water. Environ Sci Technol. 2008; 42:321–325. [PubMed: 18350915]

Appendix: Pourbaix Diagrams

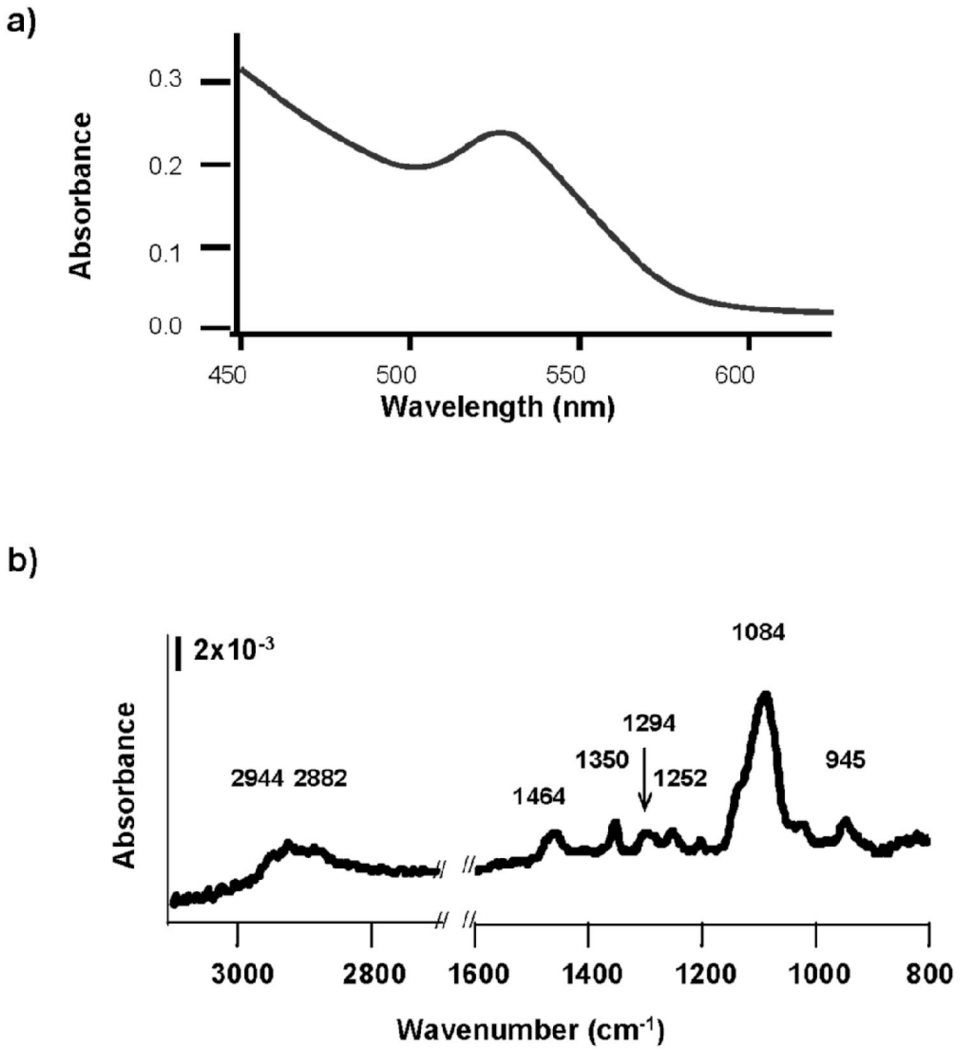

Figure 1.

Spectral characterization of as-synthesized PEGylated Cd_{core}/Zn_{shell} quantum dots (QDs). (a) Characteristic UV-Visible spectrum for PEG_{350}-QDs in water. Similar spectra were obtained for PEG_{5000}-QDs. (b) FTIR spectra of QDs ligand-exchanged with PEG_{350}.

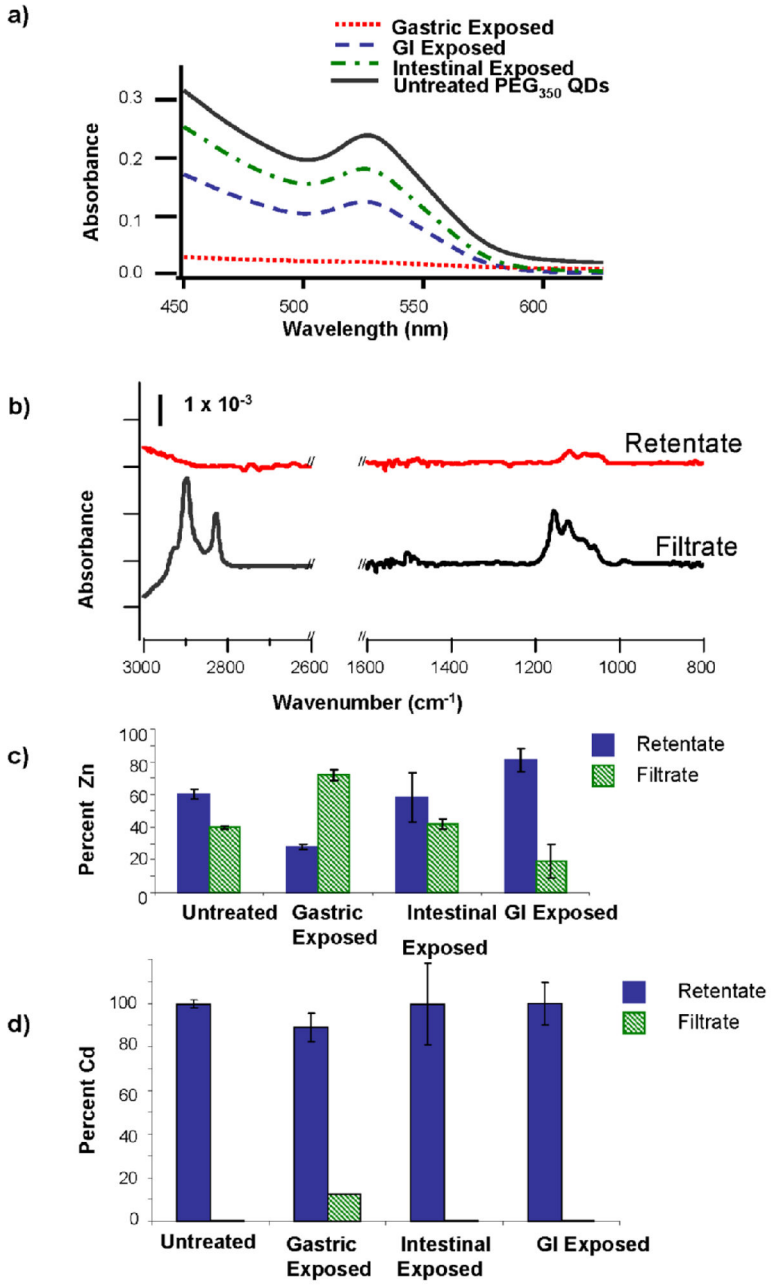

Figure 2.

(a) UV-Visible absorption spectra of PEG_{350}-QDs exposed to gastric, intestinal or gastrointestinal (GI) phase. (b) FTIR spectra of gastric exposed PEG_{350}-QDs. After exposure, solutions were separated by centrifugal filtration and analyzed for the presence of PEG_{350} ligand in the retentate (red) and filtrate (black). Percentages of (c) Zn and (d) Cd in the retentate and filtrate of PEG_{350}-QDs exposed to simulated digestive fluids. After exposure, QDs were separated from solution by centrifugal filtration, and metals concentrations determined by ICP-OES. Percentages were calculated relative to total recovered metal. Bars are means of triplicate samples; error bars represent one standard deviation.

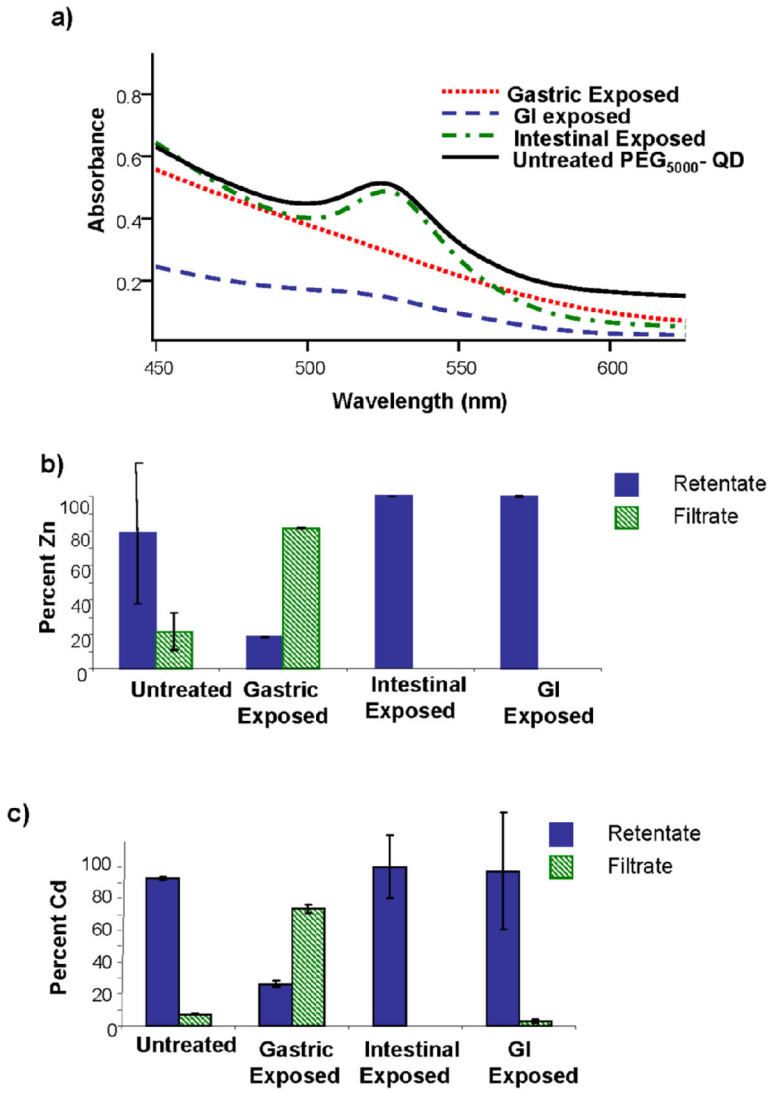

Figure 3.

(a) UV-Visible absorption spectra of PEG_{5000}-QDs following exposure to gastric, intestinal or gastrointestinal fluid exposure. Percentages of (b) Zn and (c) Cd in the retentate and filtrate of PEG_{5000}-coated QDs exposed to simulated digestive fluids. Following exposure, QDs were separated from solution by centrifugal filtration. Percentages were calculated relative to total recovered metal. Bars are means of triplicate samples; error bars represent one standard deviation.

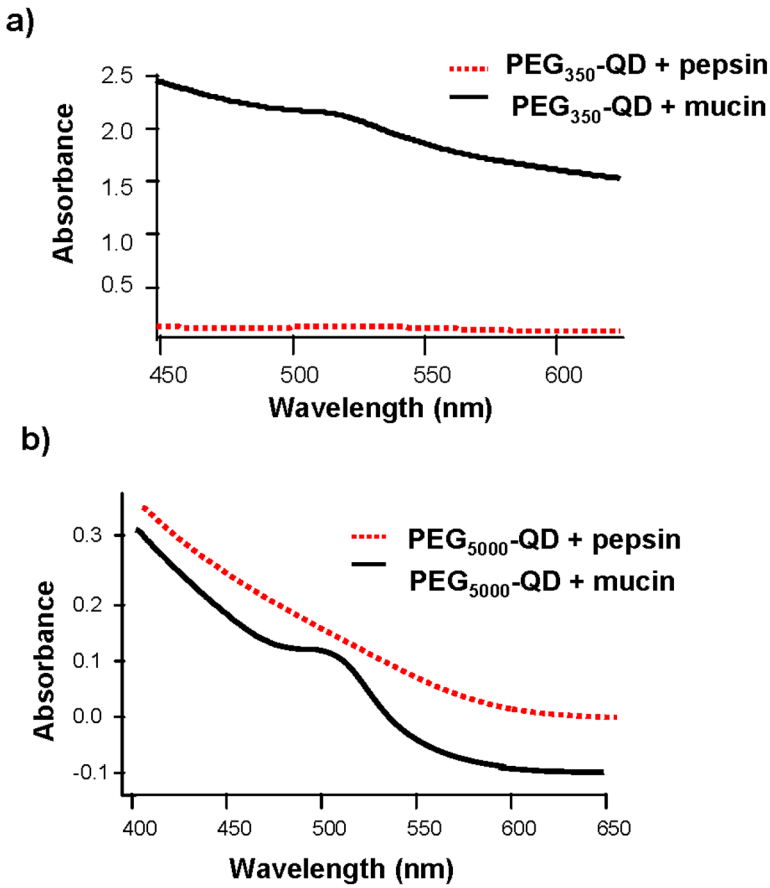

Figure 4.

UV-Visible absorption spectra of (a) PEG_{350}- and (b) PEG_{5000}-QDs following exposure to simulated gastric fluid that included gastric (glyco)proteins.

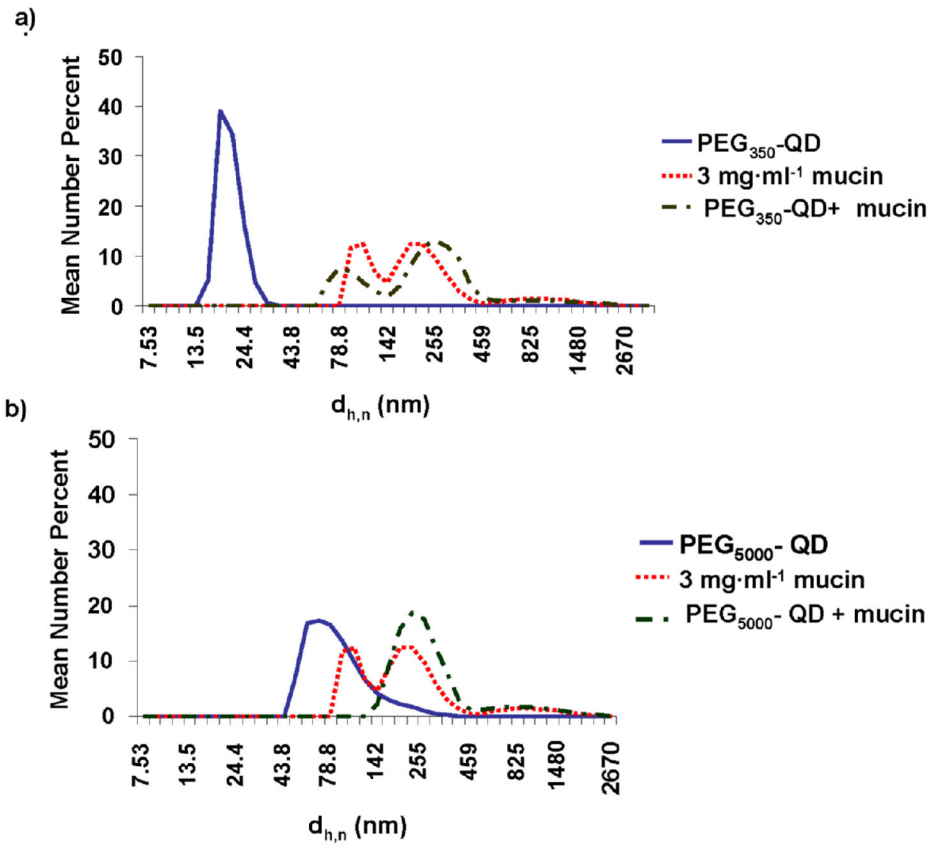

Figure 5.

PEGylated QD number distributions (averaged over 5 runs) in the absence and presence of mucin. (a) PEG_{350}-QDs and (b) PEG_{5000}-QDs.

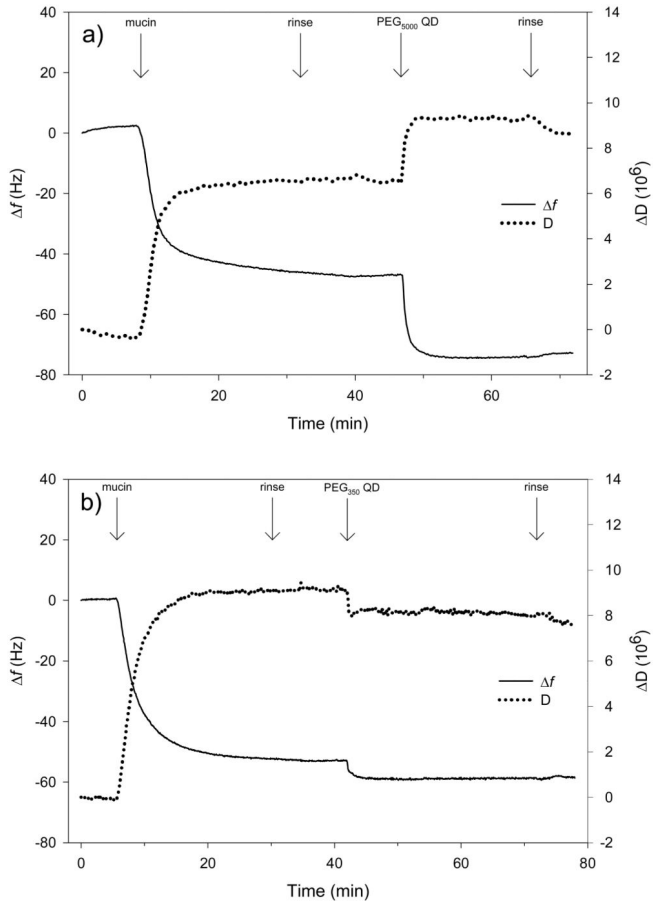

Figure 6.

Changes in frequency (Δ*f*) and dissipation (Δ*D*) recorded during QCM-D experiments using (a) PEG_{5000}- and (b) PEG_{350}-QDs. Decreases in *f* indicate an increase in deposited mass (including coupled waster). Increases in *D* correspond to increases in the viscoelasticity of the attached mass (i.e., less coupling of the vibrations of the crystal). Labels at the top of the plots indicate times when liquid phase composition was altered. Quantum dot number concentration was 2 μM (i.e. 1×10^{18} QD·L^{-1}) in 0.03 M NaCl at pH 4.

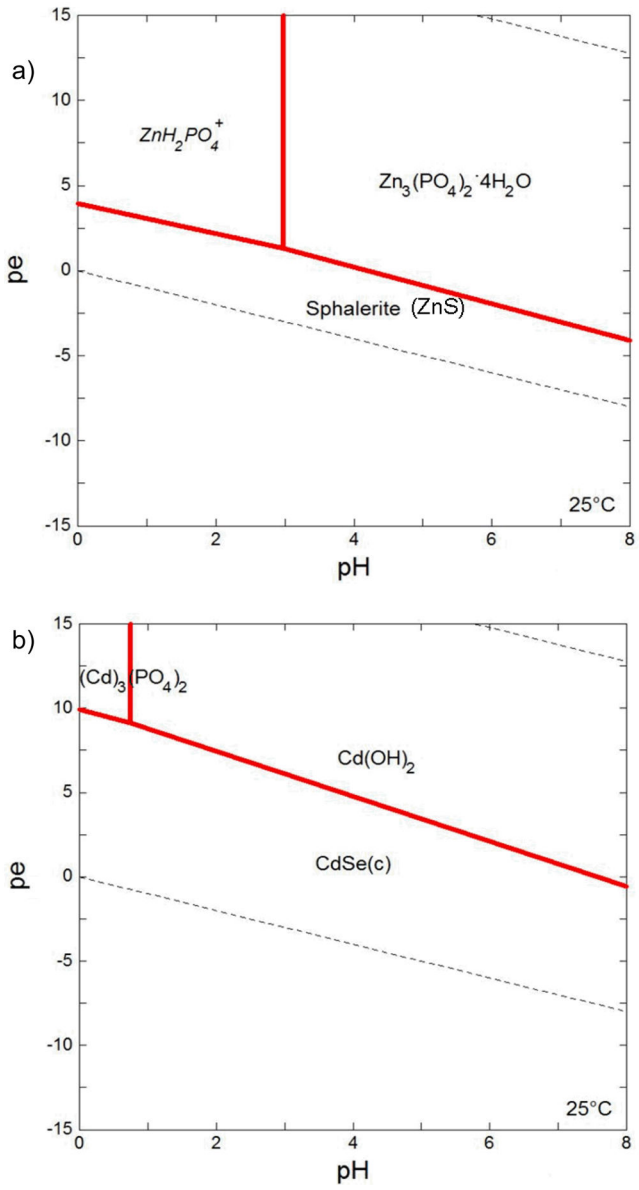

Figure 7.

pε-pH diagrams for (a) ZnS and (b) CdSe under simulated gastric conditions at 25°C. Diagrams were produced using Geochemist's Workbench v 3.0 (Bethke, 1998). Stability constants for Se, S and Zn species were from the data table for the program. Solubility products and stability constants for cadmium species were taken from Bard et al. (1985), Hankare et. al. (2006), and Stumm and Morgan (1996). The concentrations of ionic species reflected those in the simulated gastric fluids. Total amounts of Cd ($10^{-2.1}$ mole) and Zn ($10^{-7.7}$ mole) were based on concentrations measured by ICP-OES (Figures 2 and 3). As Se and Cd are present in 1:1 stoichiometry, total Se is equal to total Cd. Concentration of S was set at 10^{-5} M. (italics = dissolved species; (c) = cubic)

Table I

Compositions of the simulated gastric and intestinal fluids

Compound	Gastric (pH = 2, *I* = 0.07M) Concentration	Intestinal (pH = 7.5, *I* = 0.01M) Concentration
NaCl	0.05 M	
$KHPO_4$	0.0014 M	
KCl	0.0094 M	0.004 M
Pepsin	1 mg mL^{-1}	
Mucin	3 mg mL^{-1}	
$CaCl_2$		0.0045 M
$MgCl_2 \cdot 6\ H_2O$		0.002 M
Urea		0.005 M
Bile salts[1]		9 mg mL^{-1}
Pancreatin[2]		9 mg mL^{-1}
O_2 (aq)	0.00022 M	0.00022 M
E_H [3]	+1.02 V	+0.69 V

[1] Ox bile extract, consisting mainly of sodium glycocholate and sodium taurocholate

[2] Contains a variety of enzymes including amylase, trypsin, lipase, ribonuclease and protease.

[3] Calculated as $E_H = E_H^0 - 0.059 \cdot pH + 0.01475 \cdot \log[O_2]$ with $E_H^0 = 1.19$ V (Stumm and Morgan, 1996).

Table II

Peak assignments for poly(ethylene glycol) bound to a surface (Harder et al., 1998). (s = shoulder, EG = ethylene glycol)

Wavenumber (cm^{-1})	Assignment
2935s	CH_3 Asymmetric Stretch
2856	EG-CH_2 stretch broad
2181s	Alkyl CH_2 stretch
1452	EG-CH_2 scissor
1350	EG-CH_2 wag
1294	EG-CH_2 twist
1246	EG-CH_2 twist
1199	EG-OCH_3 rocking
1140	C-O, C-C stretch
1095	C-O,C-C stretch
1028	C-O, C-C stretch
945	EG-CH_2 rocking